Chemical Engineering Journal 468 (2023) 143514

Contents lists available at ScienceDirect

Chemical Engineering Journal

journal homepage: www.elsevier.com/locate/cej

Flexible capacitive sensor based on Miura-ori structure

Hong Sun [a], Yuxuan Sun [a], Chayut Buranabunwong [a], Xingxiang Li [a], Shiwu Zhang [a,*], Yong Chen [b,*], Mujun Li [a,*]

[a] Department of Precision Machinery and Precision Instrumentation, University of Science and Technology of China, Hefei 230026, People's Republic of China
[b] Epstein Department of Industrial and Systems Engineering, Viterbi School of Engineering, University of Southern California, Los Angeles, CA 90089, USA

ARTICLE INFO

Keywords:
Flexible capacitive pressure sensors
Miura-ori structure
Sensitivity
High stretchability
Physiological signal monitoring

ABSTRACT

Flexible capacitive pressure sensors have been widely used in applications ranging from healthcare monitoring to human − machine interaction. However, it remains a huge challenge to overcome the sensitivity attenuation with increasing pressure, as well as maintain sensing performance at high stretching. Herein, inspired by the Miura-ori structure, a Symmetrical Miura-ori Capacitive sensor (SMC sensor) is proposed to realize a positive correlation between sensitivity and pressure within a tunable pressure range, which can be adjusted by modifying the SMC sensor structures. The capacitance is determined through the synergistic effect of distance and opposite area between electrodes conformal to the Miura-ori structure. The SMC sensor exhibits a maximum sensitivity of 0.648 kPa^{-1} and high stability over 1000 cycles of compression and stretching. Furthermore, the special folding model of the Miura-ori structure avoids shape attenuation in sensitivity during stretching and detects both contractive and stretched strains. These unique characteristics make the proposed sensor promising for general physiological signal monitoring, even with high stretching and environmental adaptability.

1. Introduction

Flexible capacitive pressure sensors have a wide range of applications in wearable health monitoring [1,2], biomimetic robots [3], and electronic skins [4–6] due to their advantages of construction simplicity, low temperature coefficient, low power consumption, fast response, and low detection limit. Sensitivity is one of the essential indexes used to evaluate the performance of pressure sensors. To enhance the sensitivity, researchers often add appropriate conductive fillers to improve the dielectric constant [7,8] or introduce microstructures [9–15] to improve the compression characteristics.

However, the significant attenuation of sensitivity in the high-pressure region has not been completely addressed. One reason for the dramatic decrease in sensitivity at high pressure is that the opposite area between electrodes of different structures remains constant [16,17] under pressure, while the distance variation gradually decreases because of the increasing stiffness of the sensors. A sensor with micropyramids structure in the dielectric first proposed by Bao *et al.* [18] has a high sensitivity of 0.76 kPa^{-1} at pressures less than 2 kPa. But the electrodes with a plane structure make the sensitivity drop to 0.11 kPa^{-1} when the pressure is increased from 2 to 10 kPa. Guo *et al.* [19] used a lotus leaf as a template to obtain a capacitive pressure sensor with a microneedle structure electrode, which has a sensitivity of 1.194 kPa^{-1} at pressures less than 2 kPa. But the sensitivity decreases to 0.077 kPa^{-1} as the pressure increases because of the constant opposite area between electrodes. Xiong *et al.* [20] proposed microsphere structures in the electrodes of a capacitive pressure sensor to achieve a high sensitivity of 30.2 kPa^{-1}. However, the opposite area remains constant as well, which makes the high sensitivity only maintained in the pressure range of 0–130 Pa, followed by a 64-fold decrease in sensitivity at pressures above this range. The phenomenon of sensitivity attenuation will limit the applications of sensors with environmental pressure, such as the pressure caused by water and diving suits when divers work underwater. In addition, conflicts between the high sensitivity and stretchability in capacitive pressure sensors make them difficult to apply to situations requiring large strain. Moreover, human skin or soft robots typically perform movements with substantial deformations, which require not only stretchability [21,22] but also contractibility for flexible sensors. However, there are few reports of capacitive pressure sensors with contractibility. Therefore, it is still an open challenge to develop

* Corresponding authors at: Department of Precision Machinery and Precision Instrumentation, University of Science and Technology of China, Room 707 Mechanics Building #5, Hefei 230026, People's Republic of China (Shiwu Zhang and Mujun Li); Epstein Department of Industrial and Systems Engineering, Viterbi School of Engineering, University of Southern California, Los Angeles, CA 90089, USA (Yong Chen).
E-mail addresses: swzhang@ustc.edu.cn (S. Zhang), yongchen@usc.edu (Y. Chen), lmn@ustc.edu.cn (M. Li).

https://doi.org/10.1016/j.cej.2023.143514
Received 6 March 2023; Received in revised form 21 April 2023; Accepted 11 May 2023
Available online 15 May 2023

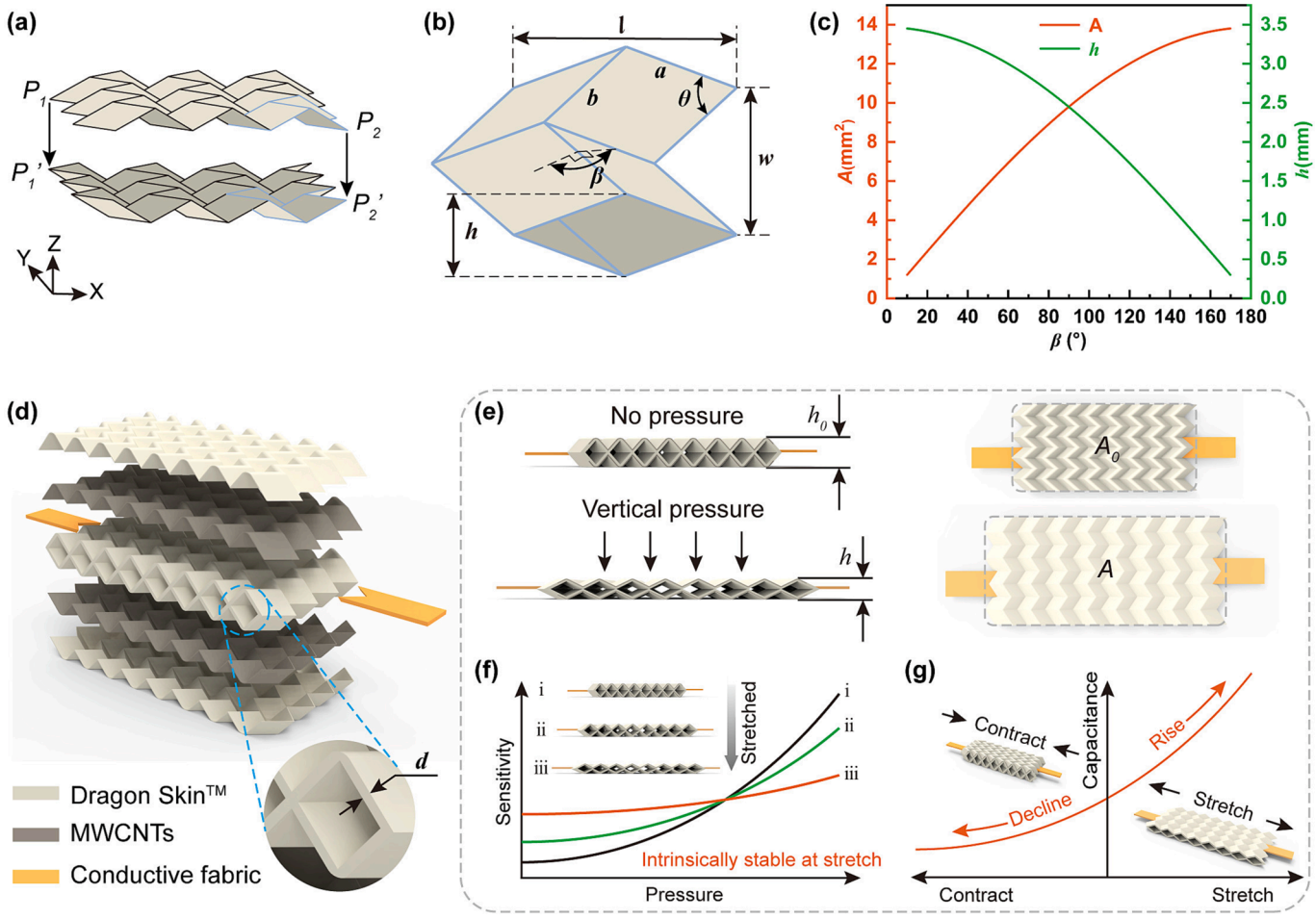

Fig. 1. Design and performance of the SMC sensor. (a) Two layers symmetric about the *X-Y* plane bonded together at the matching creases. (b) A unit cell of the symmetrical Miura-ori structure. (c) Variation in h and A (product of w and l) with dihedral angle β from 10° to 170°. (d) Structure of the SMC sensor. (e) Deformation of the capacitive sensor under vertical pressure. (f) Sensitivity of the SMC sensor while stretching. (g) Capacitance of the SMC sensor in contraction and stretching.

capacitive pressure sensors that can avoid a decrease in sensitivity with high pressure or stretching and can detect both contractive and stretched strains.

In this work, a low-cost capacitive pressure sensor is proposed based on a Miura-ori structure dielectric and electrode, which exhibits an upwards trend in sensitivity and avoids a sharp decrease under stretching. Different from the working principle of existing capacitive pressure sensors, the SMC sensor can reduce the distance h and increase the opposite area A between the electrodes when vertical pressure is applied. The special working principle makes the sensitivity gradually increase at pressures from 0 to 12 kPa and reach a maximum of 0.648 kPa^{-1} between 12 and 17 kPa. Due to the intrinsic stretchability of the Miura-ori structure, the sensor can maintain sensing performance in the stretched state and detect both contractive and stretched strains. Moreover, the capacitance of the sensor remains stable after 1000 cycles for vertical compression and horizontal stretching. The proposed sensor shows great potential for human health and movement monitoring, especially for applications that require high stretchability and environmental adaptability.

2. Experimental section

2.1. Materials

Dragon Skin™ 10 Slow and release agents (Release 200) were purchased from Smooth-On (Smooth-On, Inc., America). Graphitized hydroxyl multi-walled carbon nanotubes (MWCNTs, XFM41) as the electrodes for the sensor were purchased from XFNANO (Nanjing, China). MWCNTs are 10–20 nm in diameter and 5–30 μm in length. Conductive silver adhesive (LX50) was used to bond the electrodes to the conductive fabric. The sheet resistance of the conductive fabric is about 0.7 Ω sq^{-1}. N-hexane was acquired from Sinopharm Chemical Reagent Co. Ltd. (Shanghai, China). Sillione fluid used as a lubricant was purchased from Dow Corning. All chemicals were used as received without further purification.

2.2. Fabrication and assembly of the sensor

Concave and convex moulds with Miura-ori structures were obtained by 3D printing the related computer-aided design (CAD) models using veropurewhite material and a J750 printer (Stratasys). Part A and Part B of Dragon Skin™ were mixed at a ratio of 1:1 and cast onto concave and convex moulds sprayed with release agent. Leave in vacuum for 5 min to remove air bubbles. Then, the concave and convex moulds were tightly fitted and cured at 40 °C for 1 h. The Dragon Skin™ substrate with Miura-ori structure was obtained by peeling it off from the moulds.

MWCNTs were physically dispersed in n-hexane with an ultrasonic material disperser (LC-JY92-IIN, 240 W) for 45 min. The concentration of MWCNTs in n-hexane was 5 mg mL^{-1}. The dispersed MWCNTs were uniformly sprayed using a spray gun (W-101) on the surface of the Dragon Skin™ substrate with a Miura-ori structure and then volatilized n-hexane at 80 °C for 10 min to form electrodes. The sheet resistance of the MWCNTs electrode is about 544 Ω sq^{-1}. Dragon Skin™ and n-hexane were mixed in a mass ratio of 1:5 with a planetary mixer (ARE-310,

Thinky Company) at 2000 rpm for 3 min. The diluted Dragon Skin™ was sprayed on the electrodes and cured at 80 °C for 10 min to form encapsulation. A long strip of conductive fabric was used as a wire, which was bonded to the electrodes with conductive silver glue.

By repeating the above steps, two encapsulated Miura-ori structures with an electrode and wire were obtained. A small amount of Dragon Skin™ was evenly coated on the valley crease lines of the two prepared Miura-ori structures. Through the coordination of two concave moulds, the mountains of the two Miura-ori structures were aligned and cured at 40℃ for 1 h to form a symmetrical Miura-ori structure. Accordingly, a complete SMC sensor can be obtained.

2.3. Characterization and measurements

The capacitance of the SMC sensor was measured with a Keysight E4980AL inductance capacitance and resistance (LCR) meter at a frequency of 1 kHz and an oscillator voltage level of 1 V without dc bias. All stretching and compression tests were performed with table-top universal testing instruments (EZ Test, SHIMADZU) used in stretching and compression modes. For cyclic loading/unloading tests, the sample was placed on the testing system, and a preselected constant pressure or displacement was repeatedly loaded and released while the electrical signals were recorded. During compression testing, we used a lubricant between the sample and top/bottom plates to ensure proper mechanical deformation of the samples. The microstructures of the samples were observed by a field emission scanning electron microscope (Genimi SEM 500) operated at 3 kV.

2.4. Finite element analysis method

3D models were constructed using SolidWorks, and numerical simulations were performed using COMSOL Multiphysics (V5.3a). Due to the symmetrical condition of the model, only half of a unit was considered. The dielectric thicknesses d are 0.15 mm, 0.2 mm, 0.25 mm, 0.3 mm, and 0.35 mm. The initial dihedral angles β_0 are 20°, 60°, 90°, and 120°, respectively. The side lengths a and b of the parallelograms constituting the Miura-ori structure are both 2 mm. The upper and lower plates make the model located inside the plate when it is compression deformed to make the simulation consistent with the experimental environment. The lower plate is fixed, and vertical pressure is applied to the upper plate. The symmetrical Miura-ori structure with five elements was used for the contractive and stretched strain simulation. One end was given a fixed constraint, and the other end was stretched or contracted by different displacements. Contact pairs were set at the places that would be contacted to prevent penetration. To improve the numerical accuracy of the model, finer meshes were used for the contact area.

3. Results and discussion

3.1. Design of the SMC sensor

Fig. 1**a** illustrates two layers of the Miura-ori structure assembled symmetrically with the corresponding valley creases bonded together one by one. The resulting structure is called the symmetrical Miura-ori structure [23,24]. Fig. 1**b** shows a unit cell of the symmetrical Miura-ori structure. The sides of the parallelogram and the acute angle between the two sides are denoted by a, b, and θ, respectively. The folding degree of the Miura-ori structure is determined by the dihedral angle β. The height h, width w, and length l of a unit cell can be expressed as

$$h = 2a\cos\frac{\arccos(\sin^2\theta\cos\beta - \cos^2\theta)}{2} \tag{1}$$

$$w = 2b\sqrt{1 - \frac{\cos^2\theta}{\sin^2\frac{\beta}{2}\sin^2\theta + \cos^2\theta}} \tag{2}$$

$$l = 2a\sqrt{\sin^2\frac{\beta}{2}\sin^2\theta + \cos^2\theta} \tag{3}$$

Here, considering the convenience of calculation, a and b are set to 2 mm, and θ is set to 60°. When applying a vertical pressure, the folding degree of the symmetrical Miura-ori structure decreases, resulting in changes in the height h, width w, and length l. Fig. 1**c** shows variation in h and A (product of w and l) with dihedral angle β from 10° to 170°. It can be seen that h decreases and A increases with the reduction in folding degree. The SMC sensor is formed by covering the upper and lower surfaces of the symmetrical Miura-ori structure with electrodes. Fig. 1**d** shows the structure of the SMC sensor. It consists of Dragon Skin™ substrates, multi-walled carbon nanotubes (MWCNTs) electrodes, top and bottom Dragon Skin™ encapsulation, and conductive fabric. According to Fig. 1**c**, the electrodes with the Miura-ori structure can cause the distance and opposite area of the SMC sensor to change in the direction of increasing capacitance under pressure. This is the key to avoiding sensitivity decay with increasing pressure for SMC sensors. It is different from most of the existing flexible capacitive pressure sensors. Supplementary Table 1 lists the electrode structures of our SMC sensor and the existing capacitive pressure sensors, as well as the changes in opposite areas during compression deformation. It can be seen that the opposite area between electrodes of planes, microspheres, microcolumns, and microgrooves structures are almost consistent under deformation.

For the convenience of preparation, the side lengths a and b were set to 2 mm, and θ was set to 60°. The other parameters that determine the structure of the SMC sensor are the initial dihedral angle β_0 and dielectric thickness d (marked in Fig. 1**d**). The initial dihedral angle β_0 represents the dihedral angle of the SMC sensor when no pressure is applied. In order to select the optimal parameters, deformation simulation was carried out for sensor models with different initial dihedral angles and dielectric thicknesses by COMSOL. Fig. S1 shows the deformation of sensor models with different initial dihedral angles under the same pressure. It shows that the soft material with a small initial dihedral angle such as 20° will twist under pressure, which is inconsistent with the deformation of the Miura-ori structure. With the increase in the initial dihedral angle, the twist deformation will gradually disappear, but the symmetric Miura-ori structure will completely unfold under low pressure. For example, when the initial dihedral angle is 120°, the symmetric Miura-ori structure is unfolded under 10 kPa. The opposite area will not increase in the subsequent deformation, resulting in a narrower dynamic pressure range. Meanwhile, sensitivity (S) is defined as the tangent slope of the curve of the relative capacitance change with respect to the loaded pressure,

$$S = \frac{\delta(\Delta C/C_0)}{\delta P} \tag{4}$$

where C_0 and ΔC are the initial capacitance and variation in capacitance, respectively, and P denotes the imposed vertical pressure. **Formula 4** indicates that reducing C_0 can improve sensitivity. A smaller initial dihedral angle will result in a greater distance and smaller opposite area, which lead to a smaller initial capacitance C_0, and thus will improve the overall sensitivity. Therefore, we choose a moderate initial dihedral angle of 60° for our SMC sensors. Fig. S2 shows the deformation of sensor models with different dielectric thicknesses under the same pressure. The stiffness of the sensor model will decrease with a smaller thickness, resulting in easy deformation and a narrower dynamic pressure range. However, the stiffness will become higher with a larger thickness, resulting in difficult deformation and a lower sensitivity. Therefore, we choose a moderate dielectric thickness of 0.25 mm for SMC sensors.

Fig. S3 shows the fabrication of the SMC sensor. The Dragon Skin™ substrates were obtained by moulding through 3D-printed concave and convex moulds. The MWCNTs ultrasonically dispersed in n-hexane were

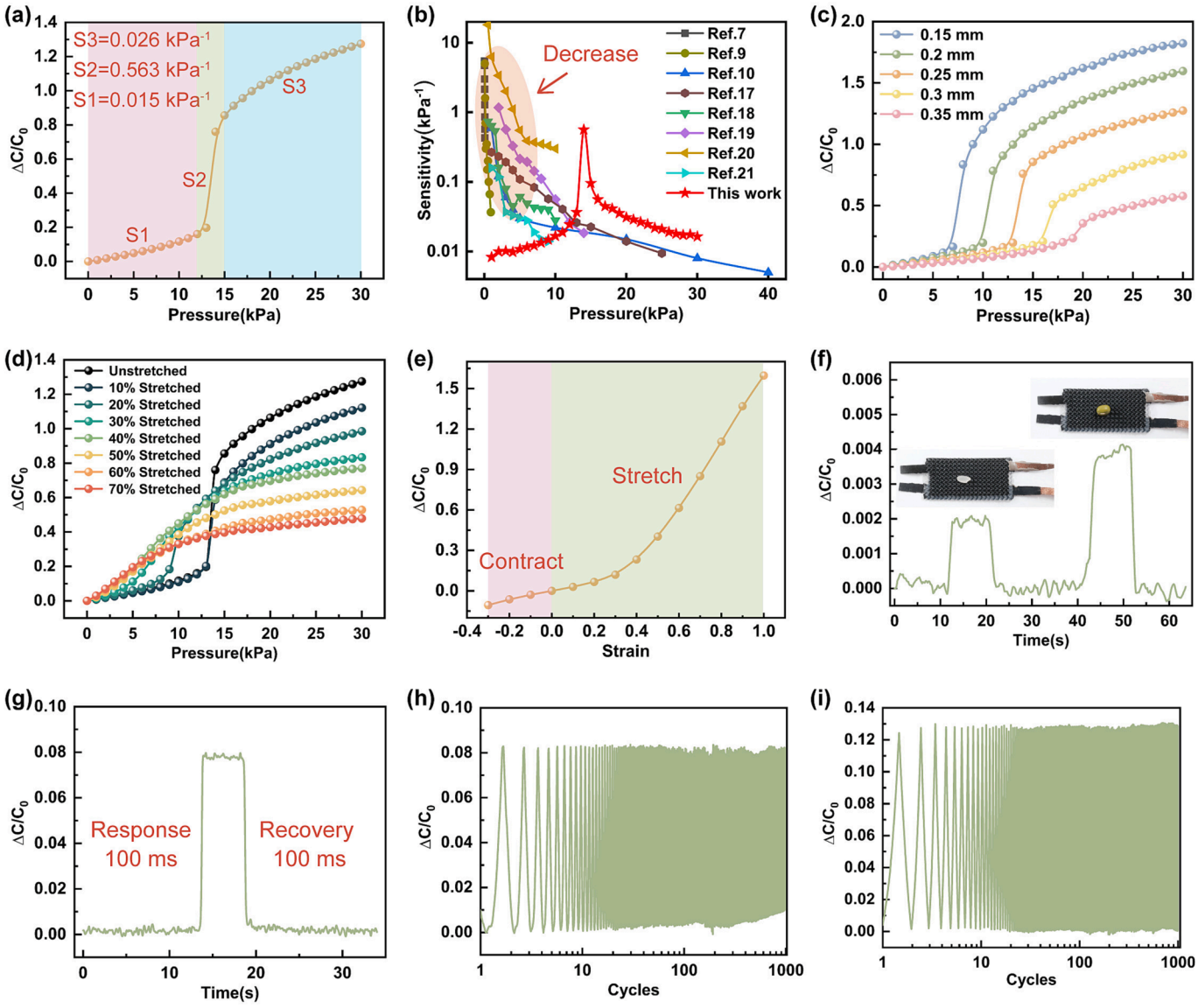

Fig. 2. Sensing performance of the SMC sensor. (a) The relationship between the variation in capacitance and the applied pressure. (b) The sensitivity trend of the SMC sensor and existing flexible capacitive pressure sensors. (c) The relationship between the variation in capacitance and the applied pressure for different dielectric thicknesses of SMC sensors. (d) The relationship between the variation in capacitance and the applied pressure at different stretching degrees. (e) Relative capacitance changes of SMC sensors under different contractive and stretched strains. (f) Capacitance response of the sensor to rice and mung bean. (g) Response and recovery times of the sensor. (h) Compression stability test (1000 cycles) of the sensor under a pressure of 1 kPa. (i) Stretching stability test (1000 cycles) of the sensor under 30% stretching.

sprayed on the surface of the substrate to form electrodes with a Miura-ori structure. To avoid contact between the upper and lower electrodes, the outer boundary of the substrate is not sprayed with MWCNTs. After the MWCNTs were dried, the conductive fabric was stuck to the electrode through conductive silver glue as the test wire. Then, a layer of Dragon Skin^{TM} dissolved in n-hexane was sprayed as an encapsulation. In order to evenly cover the electrode and encapsulation on the surface of the substrate, the substrate needs to be pre-stretched by 30% during the process of electrode and encapsulation spraying. By bonding the two fabricated above, the SMC sensor was obtained. The preparation process is cost-effective and does not require expensive materials or instruments. Significant strain is generated at the creases of the symmetrical Miura-ori structure during deformation. If granular conductive materials such as metal nanoparticles are used as electrodes, they are prone to fracture at the crease, causing instability of the sensor. Conductive materials with a high aspect ratio can alleviate the above phenomenon [19]. Therefore, low-cost MWCNTs with a high length-diameter ratio were used as electrode materials. Fig. S4**a** shows the SEM images for the top view of MWCNTs electrode surface. Fig. S4**a-ii, a-iii, and a-iv** show enlarged views of the Miura-ori structure on the peak crease, valley crease and parallelogram plane. MWCNTs are homogeneously distributed on the surface of the Dragon Skin^{TM} substrate, even in protruding peaks and sunken valleys. Fig. S4**b** shows SEM images with a cross-sectional view of the SMC sensor. Fig. S4**b-i** and **b-ii** show the full structures of symmetric Miura-ori and Miura-ori. Fig. S4**b-iii** and **b-iv** show the enlarged cross-sectional view of the peak and valley. The interface between the substrate and electrode can be clearly seen in the figure. Fig. S5 shows the resistance variation of the SMC sensor electrode with stretch cycles. The data were recorded for every 50 stretches. After 5000 cycles of stretching 50%, the resistance of the electrode did not change significantly, indicating that the electrode obtained by spraying MWCNTs is stable. It should be noted that due to the encapsulation covering the surface of the electrode and the loss at the connection between the electrode and conductive fabric, the resistance in Fig. S5 is

larger than the sheet resistance of the electrode.

The electrode of the Miura-ori structure enables SMC sensors to have the following three special characteristics. First, the SMC sensor avoids sensitivity attenuation with increasing pressure. The distance decreases while the opposite area increases between electrodes under pressure. This is the key for SMC sensors to avoid sensitivity attenuation, as shown in Fig. 1**e**. Second, it avoids rapid attenuation of sensitivity while stretching. As shown in Fig. 1**f**, with increasing stretching degree, although the maximum sensitivity decreases, the overall sensitivity tends to be stable as the minimum sensitivity increases. Third, the SMC sensor responds capacitively to both horizontal contractive and stretched strains. As shown in Fig. 1**g**, contractive strain increases the capacitance, while stretched strain leads to a decrease in the capacitance of the sensor.

3.2. Sensing properties of the SMC sensor

Fig. 2**a** shows the relative capacitance changes obtained experimentally under various vertical pressures. Within the pressure ranges of 0–12 kPa, 12–15 kPa, and 15–30 kPa, the sensitivity of the SMC sensor is 0.015 kPa^{-1}, 0.563 kPa^{-1}, and 0.026 kPa^{-1}, respectively. In the range from 0 to 14 kPa, the sensitivity of the SMC sensor increases with pressure. Here, we define this pressure range as the positive range. The sensitivity of most existing flexible capacitive pressure sensors generally decreases with increasing pressure, as shown in Fig. 2**b**. Without considering the dielectric constant ε, the sensitivity S related to the opposite area A and distance h can be given by

$$S = \frac{\frac{A}{A_0}\cdot\frac{h_0}{h} - 1}{\delta P} \tag{5}$$

Where A_0 and h_0, A and h represent the opposite area and distance before and after applying pressure, respectively. Fig. S6 shows the simulation deformation of the SMC sensor under different pressures. A reasonable explanation for the special sensitivity trend of the SMC sensor can be provided by **Formula 5** and Fig. S6. At low pressures from 0 to 5 kPa, the sensor is difficult to compress, and the sensitivity rises slowly due to the small change in distance h and opposite area A. At pressures from 5 to 15 kPa, the sensor is more prone to compression. The distance h and opposite area A change rapidly, making the sensitivity rise quickly. At pressures from 15 to 30 kPa, the stiffness of the SMC sensor increases when most of the air in the sensor has been squeezed, making the deformation gradually difficult. The distance h decreases slowly, while the opposite area A is almost constant, making the sensitivity decrease as with most existing sensors. Fig. S7 shows the capacitive response of the SMC sensor to a low pressure of 10 Pa under different environmental pressures. The capacitance response under a 13 kPa environmental pressure is much higher than the other two. The excellent sensing performance of the sensor under environmental pressure was verified. Fig. 2**c** shows the relative capacitance changes of SMC sensors with different dielectric thicknesses d under various vertical pressures. As the thickness increases, the positive ranges of sensitivity are 0–8 kPa, 0–11 kPa, 0–14 kPa, 0–17 kPa, and 0–20 kPa, respectively. This indicates that the sensitivity positive range of the SMC sensor can be adjusted by dielectric thickness d. To further improve the sensitivity of SMC sensors, 0.5 wt% MWCNTs were added to Dragon Skin™ to obtain a higher dielectric constant. The preparation of the composite dielectric is described in **Note 1** of the Supplementary Material. First, sensitivities are tested on circular capacitive sensors with the dielectric of pure Dragon Skin™ and the composite dielectric, as shown in Fig. S8**a**. The diameter and thickness of the circular capacitive sensor are 1 cm and 1 mm, respectively. It shows that the sensitivity of the composite dielectric capacitive sensor is approximately twice that of the pure Dragon Skin™ dielectric capacitive sensor. Next, sensitivities are measured on SMC sensors with the dielectric of pure Dragon Skin™ and the composite dielectric, as shown in Fig. S8**b**. It shows that sensitivities are improved over the entire pressure range, especially in the high-pressure region where it is increased by two times. Meanwhile, the composite dielectric extends the pressure range with maximum sensitivity from 12 to 15 kPa to 12–17 kPa. Supplementary Table 2 lists the sensitivities and dynamic ranges of the SMC sensor and existing capacitive sensors with the same scale [25–29]. Compared with existing sensors at the same scale, the SMC sensor has good sensitivity and dynamic range.

Fig. 2**d** shows the relative capacitance changes with pressure at stretching degrees from 0 to 70% of the SMC sensor. As the degree of stretching increases, the inflection points of the curves gradually move in the direction of low pressure. When the degree of stretching is less than 20%, the sensitivity first increases and then decreases, similar to the trend when no stretching is applied. As the stretching degree increases, the maximum sensitivity decreases, the minimum sensitivity increases, and the overall sensitivity tends to stabilize. Optical images of SMC sensors with different stretching degrees are shown in Fig. S9. The stretching of the sensor is caused by the crease unfolding of the symmetrical Miura-ori structure, rather than the strain of the material itself. As shown in Fig. S10, at 50% stretched strain, the stress is mainly concentrated at the crease of the symmetric Miura-ori structure. Fig. S11 shows the capacitance response of the sensor to detect 1 kPa pressure without stretching and with a stretching degree of 100%. The capacitance response at 100% stretching is larger than that without stretching. This indicates that the sensitivity of the SMC sensor after 100% stretching is higher than that without stretching, which is consistent with the results in Fig. 2**d**. Fig. 2**e** and Fig. S12 show the relative capacitance changes and deformation of SMC sensors under different contractive or stretched strains. When the SMC sensor contracts, the distance between the electrodes increases, and the opposite area decreases, resulting in a capacitance decrease. Similarly, the capacitance will increase when the sensor is stretched. Therefore, SMC sensors have the ability to detect contractive and stretched strains.

To investigate the detection limit of the capacitive sensor, rice with a mass of approximately 20 mg and mung bean with a mass of approximately 60 mg were placed on the sensor surface. As shown in Fig. 2**f**, the sensor has a significant capacitance response for a single rice and mung bean. The minimum limit of detection of the SMC sensor is about 20 mg, approximately equivalent to 5 Pa. We investigated the response and recovery time of the SMC sensor by loading and unloading a pressure of 1 kPa on the sensor, as shown in Fig. 2**g** and Fig. S13. The excellent elasticity of the Dragon Skin™ and the hollow structure also enables a fast response and recovery time of approximately 100 ms. Furthermore, the compression stability of the sensor was evaluated by cyclically loading and unloading a pressure of 1 kPa for 1000 cycles, as shown in Fig. 2**h**. The stretching stability of the SMC sensor was evaluated by performing a stretch cycle test in the stretch mode of the universal testing instrument, as shown in Fig. 2**i**. The sensor was stretched by 30% and then released to its original length for 1000 cycles. Fig. S14 and Fig. S15 show the capacitance response curves of the SMC sensor during the initial and final stages of the compression and stretching cycle testing. During the process of loading and unloading, the output capacitance signal of the sensor remains stable. After 1000 cycles, the attenuation of the capacitance signal can be negligible, which indicates excellent compression and stretching stability of the SMC sensor.

In addition, the Miura-ori structure can also be designed as an array of sensors to detect pressure distribution, named Symmetrical Miura-ori Capacitive Array sensor (SMCA sensor). The structure of the SMCA sensor is shown in Fig. S16**a**. The ability of the SMCA sensor to detect the pressure distribution was verified through simulation. In the simulations, we apply pressure F1 on areas A2 and A8, and apply pressure F2 on areas A4 and A6, where F2 = 2F1. The deformation and capacitance response obtained from the simulation are shown in Fig. S16**b**. The results show that the SMCA sensor can detect the pressure distribution well.

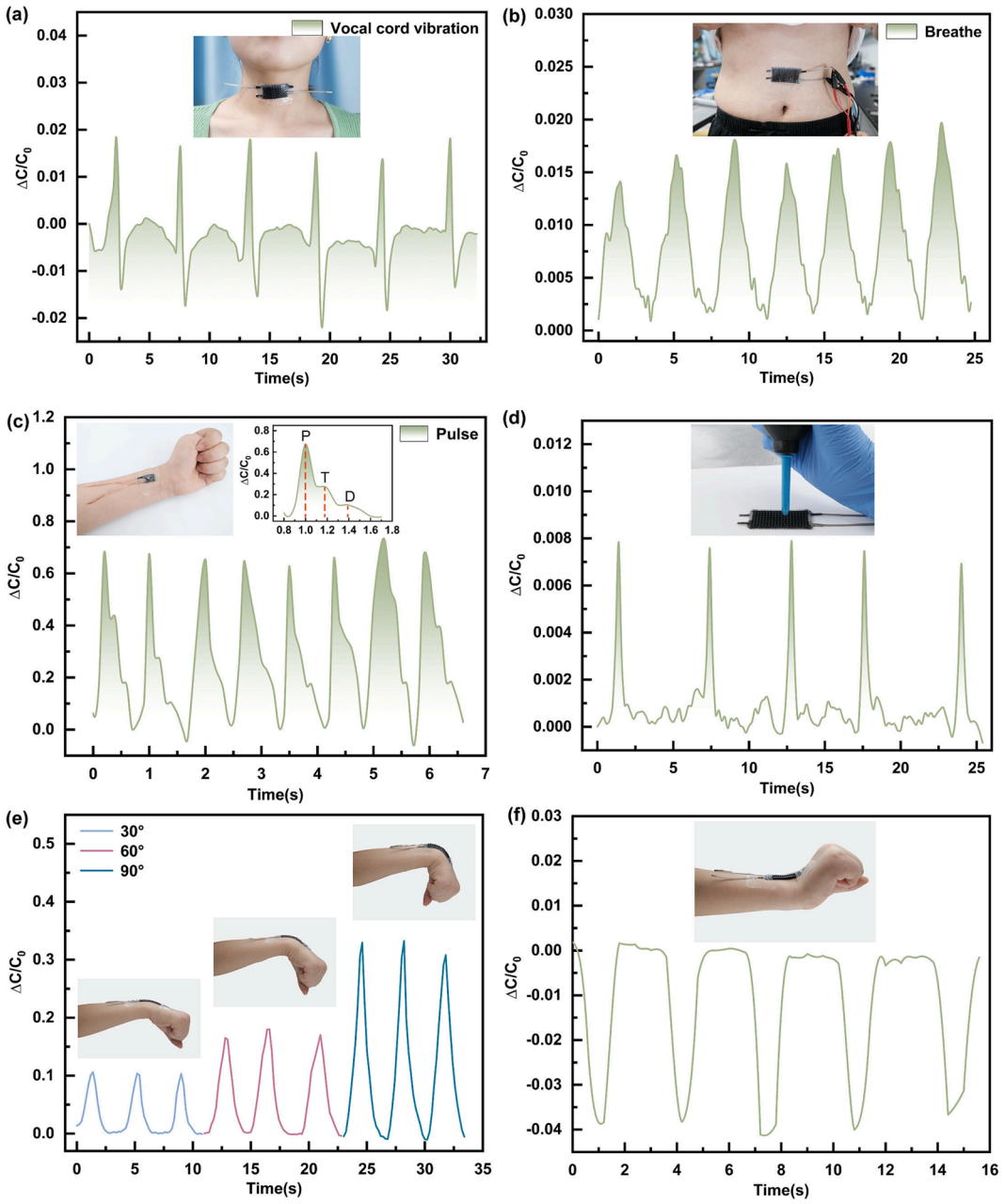

Fig. 3. Application of SMC sensors in human signal detection. (a) Detection of vocal cord vibration signals caused by the "sensor". (b) Detection of the breath rate by attaching the sensor to the abdomen. (c) Detection of the pulse signal on the wrist (the enlarged illustration is a magnified view of the pulse vibration waveform). (d) Detection of repeated air flow. (e) Detection of wrist bending downwards at 30°, 60°, and 90°. (f) Detection of wrist bending upwards motions.

3.3. Practical applications of the SMC sensor

Fig. S17 shows that the strain in the *X* direction is positively correlated with that in the *Y* direction during the deformation of the symmetrical Mirua-ori structure, which shows a negative Poisson's ratio. Taking advantage of the excellent sensing performance and negative Poisson's ratio, the SMC sensor can be used as a wearable device to detect human physiological signals conformally with the skin surface [30]. For example, speech signals are caused by movements of neck muscles and vibrations of the vocal cords. To demonstrate its potential for speech signal recognition, the SMC sensor was attached to the neck of the experimenter. Video S1 demonstrates the real-time information on the experimenter and capacitance response of the SMC sensor. When the experimenter speaks the word "sensor", the capacitance of the SMC sensor first increases and then decreases. Fig. 3**a** shows a segment of the capacitance signal in the video. The output signal has good consistency, indicating that the sensor can clearly recognize human voice signals. Detecting the respiratory rate is significant for conditions such as asthma and sleep apnea. Fig. 3**b** shows the respiratory signal obtained by attaching the sensor to the experimenter's abdomen. The results show that the frequency and amplitude of the output signals have excellent consistency, indicating their potential application in monitoring respiratory abnormalities. Heart rate is closely related to heart disease, so the monitoring of daily heart rate is particularly important. Fig. 3**c** shows the real-time pulse measured by attaching the sensor to the experimenter's wrist, with a frequency of approximately 75 beats per minute. The inset in Fig. 3**c** shows the characteristic peaks of pulse waves, including percussion (*P*), tidal (*T*), and dicrotic (*D*). Fig. 3**d** shows the real-time response of the sensor to airflow. When squeezing the rubber suction bulb, the airflow transmits pressure to the sensor, causing a

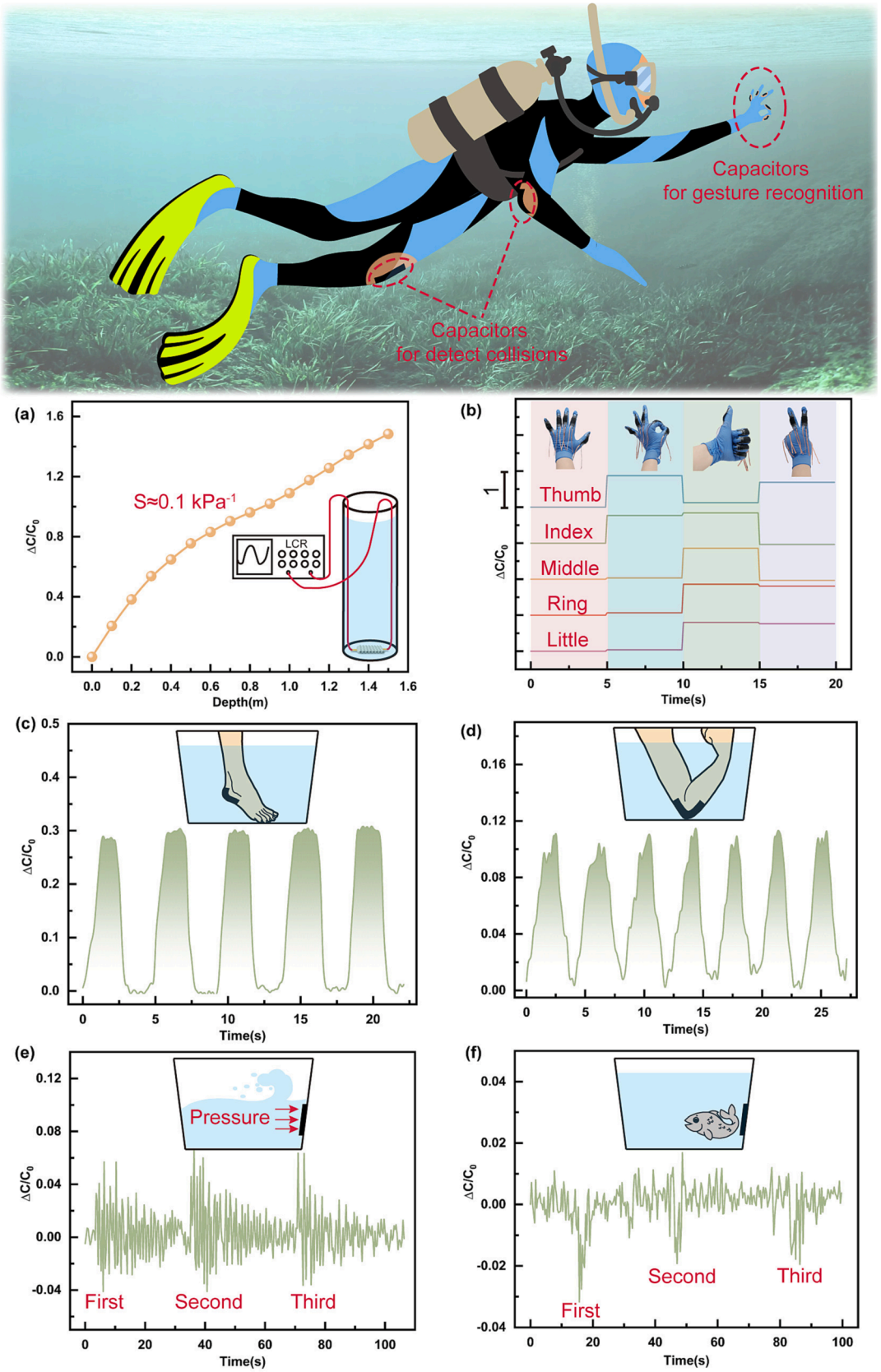

Fig. 4. The application of SMC sensors underwater. (a) Capacitance response of the sensor to water pressure. (b) Capacitance signals at different gestures. (c) Capacitance response of touch where the SMC sensor was attached to the feet under water. (d) Capacitance response of touch where the SMC sensor was attached to the bending elbow under water. (e) Capacitance response of the SMC sensor when a wave shock approached. (f) Capacitance response of the SMC sensor when fish are swimming by.

significant increase in capacitance. This demonstrates the potential applications of the SMC sensor in airflow detection, such as wind direction and speed. Fig. 2**e** shows the ability of the capacitive sensor to detect both contractive and stretched strains. Based on this, the SMC sensor can detect the bending signal both downwards and upwards at the human joint. We attached the sensor on the outside wrist to detect the bending movement. As shown in Fig. 3**e**, when the wrist was bent downwards, the sensor was stretched to output an increased capacitance signal. The sensor can also identify the degree of wrist bending. When the wrist is bent by 30°, 60°, and 90°, the sensor outputs a capacitance signal that increases sequentially. When the wrist was bent upwards, the sensor contracted, producing a reduced capacitance signal, as shown in Fig. 3**f**. The experimental processes are shown in Video S2. This will expand the applications of capacitive pressure sensors to a certain extent, such as omnidirectional detection of the joint motion of the human body.

The positive correlation between the sensitivity and pressure of the SMC sensor is suitable for the detection of the presence of environmental pressure, such as the related monitoring of divers while they are working underwater. Both the tight-fitting wetsuit and water pressure will cause environmental pressure on the sensor while attaching it to the diver's body for underwater monitoring. To demonstrate the applicability of the proposed sensor in this scenario, the SMC sensor was placed in a waterproof plastic bag to simulate the environmental pressure on the sensor by a wetsuit. The packaged sensor was placed in a bucket with a depth of 1.5 m, and water was gradually added into the bucket to simulate the water depth. With this setup, the water pressure ranges from 0 to 15 kPa. The experimental setup is shown in Fig. S18**a**, and the experimental results are shown in Fig. 4**a**. The relative capacitance increases with increasing water pressure. The sensitivity is approximately 0.1 kPa^{-1}, which is greater than the sensitivity of the sensor under normal conditions for the same pressure range. This shows that the proposed sensor can detect the dive depth of the diver. To work underwater, divers need to transmit signals from underwater to the surface. The sensors are attached to the diver's finger joints so that signals can be generated through different hand gestures. When the hand makes a specified gesture, the bending of the finger joints leads to the stretching of the sensor, and the relative capacitance outputs different values. Fig. 4**b** demonstrates the application of the SMC sensor for gesture recognition. First, the five fingers were straightened, and the output signals of the five sensors were in a low initial state. After that, the gestures of "OK", "Good", and "Yeah" were made, and the obtained signal can well reflect the gesture change. In addition, divers may be hurt by hitting rocks while working underwater. The proposed sensors were attached to the bottom of the diver's feet, elbows, and knees, which can sensitively sense the touch of the rocks, so an alarm can be sent to the divers to protect themselves. Fig. S18**b** shows the waterproof treatment of the SMC sensor for reef collision detection. Fig. 4**c** shows the capacitance output signal obtained by the foot touching the bottom of the container containing water. The capacitance of each touch increases significantly, indicating that the sensor can perceive the external impacts well. Taking advantage of the fact that the proposed sensor can work well under stretching, the sensor can be attached to the outside of the straightened elbow and can detect contact with the reef when the elbow is straightened or bent. Fig. 4**d** shows the relevant test results. The output capacitance signal changes significantly with each touch of the elbow. This shows that the sensor can sense external touch in the stretched state. The experimental processes are shown in Video S3 and Video S4. In addition, the proposed sensor can also be used for underwater fish detection. When deployed underwater, the sensor will be affected by many factors, including wave shocks and fish movements. As shown in Fig. 4**e,** when a wave shock approached (here, we moved a glass plate in the water to generate shocks to simulate water waves), the resulting water pressure caused the capacitance of the sensor to fluctuate up and down. While a fish swims approaching the sensors, the electric field around the capacitor will be affected, resulting in a decrease in the capacitance, as shown in Fig. 4**f**. By utilizing these different responses of our sensors to wave shocks and fish movement, it is possible to distinguish between the wave impact and the movement of fish swimming by. This may be useful for studying fish behaviours and provide potential methods to understand the activities and distribution of fish. The detailed experimental processes are shown in Video S5.

4. Conclusion

In this work, we present a unique flexible capacitive pressure sensor based on the Miura-ori structure dielectric and electrode. A low-cost method has been proposed in which the SMC sensor is constructed by moulding using 3D-printed moulds and sprayed with flexible MWCNTs electrodes. Based on finite element analysis simulations and experimental results, the special deformation of the symmetrical Miura-ori structure makes the sensitivity of the SMC sensor positively correlated with pressure, which is key to avoiding a sharp decrease during stretching as well. In addition, the SMC sensor has excellent scalability to detect both contractive and stretched strains. It also has a high sensitivity of 0.648 kPa^{-1}, a low detection limit of 5 Pa, a fast response/recovery time of 100 ms, and excellent stability for over 1000 cycles of compression and stretching. The architecture based on the Miura-ori structure may open a new route for constructing high-performance flexible capacitive pressure sensors in the future. We demonstrate its promising potential in applications such as omnidirectional human body monitoring and movement detection.

Declaration of Competing Interest

The authors declare that they have no known competing financial interests or personal relationships that could have appeared to influence the work reported in this paper.

Data availability

Data will be made available on request.

Acknowledgements

This work was supported by funding from the National Key Research and Development Program of China (Grant No. 2020YFA0710100), the Natural Science Foundation of Anhui Province (Grant No. 2108085ME170), the Key Research and Development Program of Anhui Province (Grant No. 2022a05020008), the National Natural Science Foundation of China (Grant No. 51475442), the Joint Funds from Hefei National Synchrotron Radiation Laboratory (Grant No. KY2090000068), and partially carried out at the USTC Center for Micro and Nanoscale Research and Fabrication, and Engineering Practice Center, University of Science and Technology of China.

Appendix A. Supplementary data

Supplementary data to this article can be found online at https://doi.org/10.1016/j.cej.2023.143514.

References

[1] M. Yuan, F. Luo, Z. Wang, J. Yu, H. Li, X. Chen, Smart wearable band-aid integrated with high-performance micro-supercapacitor, humidity and pressure sensor for multifunctional monitoring, Chem. Eng. J. 453 (2023) 139898.
[2] J. Ji, C.P. Zhang, S.H. Yang, Y.Z. Liu, J.L. Wang, Z.Y. Shi, High Sensitivity and a Wide Sensing Range Flexible Strain Sensor Based on the V-Groove/Wrinkles Hierarchical Array, ACS Appl. Mater. Inter. 14 (20) (2022) 24059–24066, https://doi.org/10.1021/acsami.2c04773.
[3] K. He, Y.Q. Liu, M. Wang, G. Chen, Y. Jiang, J.C. Yu, C.J. Wan, D.P. Qi, M. Xiao, W. R. Leow, H. Yang, M. Antonietti, X.D. Chen, A.A.S.R. Arc, Adv. Mater. 32 (4) (2020), https://doi.org/10.1002/adma.201905399.
[4] C. Hou, Z. Xu, W.u. Qiu, R. Wu, Y. Wang, Q. Xu, X.Y. Liu, W. Guo, A Biodegradable and Stretchable Protein-Based Sensor as Artificial Electronic Skin for Human Motion Detection, Small 15 (11) (2019) 1805084.

[5] H. Luo, Y. Shen, Z. Liao, X. Yang, B. Gao, B. He, Spidroin Composite Biomimetic Multifunctional Skin with Meta-Structure, Adv. Mater. Technol.-Us 7 (6) (2022) 2101097.
[6] M. Zhu, M. Lou, I. Abdalla, J. Yu, Z. Li, B. Ding, Highly shape adaptive fiber based electronic skin for sensitive joint motion monitoring and tactile sensing, Nano Energy 69 (2020) 104429.
[7] J. Wang, J.T. Jiu, M. Nogi, T. Sugahara, S. Nagao, H. Koga, P. He, K. Suganuma, A highly sensitive and flexible pressure sensor with electrodes and elastomeric interlayer containing silver nanowires, Nanoscale 7 (7) (2015) 2926–2932, https://doi.org/10.1039/c4nr06494a.
[8] A. Chhetry, S. Sharma, H. Yoon, S. Ko, J.Y. Park, Enhanced Sensitivity of Capacitive Pressure and Strain Sensor Based on CaCu3Ti4O12 Wrapped Hybrid Sponge for Wearable Applications, Adv. Funct. Mater. 30 (31) (2020) 1910020.
[9] H. Niu, S. Gao, W. Yue, Y. Li, W. Zhou, H. Liu, Highly Morphology-Controllable and Highly Sensitive Capacitive Tactile Sensor Based on Epidermis-Dermis-Inspired Interlocked Asymmetric-Nanocone Arrays for Detection of Tiny Pressure, Small 16 (4) (2020) 1904774.
[10] Y.Q. Liu, J.R. Zhang, D.D. Han, Y.L. Zhang, H.B. Sun, Versatile Electronic Skins with Biomimetic Micronanostructures Fabricated Using Natural Reed Leaves as Templates, ACS Appl. Mater. Inter. 11 (41) (2019) 38084–38091, https://doi.org/10.1021/acsami.9b14135.
[11] J.H. Zhang, Z.T. Li, J. Xu, J. Li, K. Yan, W. Cheng, M. Xin, T.S. Zhu, J.H. Du, S. X. Chen, X.M. An, Z. Zhou, L.Y. Cheng, S. Ying, J. Zhang, X.X. Gao, Q.H. Zhang, X. D. Jia, Y. Shi, L.J. Pan, Versatile self-assembled electrospun micro-pyramid arrays for high-performance on-skin devices with minimal sensory interference, Nat. Commun. 13 (1) (2022), https://doi.org/10.1038/s41467-022-33454-y.
[12] J.C. Yang, J.O. Kim, J. Oh, S.Y. Kwon, J.Y. Sim, D.W. Kim, H.B. Choi, S. Park, Microstructured Porous Pyramid-Based Ultrahigh Sensitive Pressure Sensor Insensitive to Strain and Temperature, ACS Appl. Mater. Inter. 11 (21) (2019) 19472–19480, https://doi.org/10.1021/acsami.9b03261.
[13] L. Pan, L. Han, H. Liu, J. Zhao, Y. Dong, X. Wang, Flexible sensor based on Hair-like microstructured ionic hydrogel with high sensitivity for pulse wave detection, Chem. Eng. J. 450 (2022) 137929.
[14] S. Yang, C. Zhang, J. Ji, Y. Liu, J. Wang, Z. Shi, Performance Improvement of Flexible Pressure Sensor Based on Ordered Hierarchical Structure Array, Adv. Mater. Technol.-Us 7 (11) (2022) 2200309.
[15] B.Q. Nie, J.L. Geng, T. Yao, Y.H. Miao, Y.Q. Zhang, X.J. Chen, J. Liu, Sensing arbitrary contact forces with a flexible porous dielectric elastomer, Mater. Horiz. 8 (3) (2021) 962–971, https://doi.org/10.1039/d0mh01359e.
[16] Y. Wan, Z. Qiu, J. Huang, J. Yang, Q.i. Wang, P. Lu, J. Yang, J. Zhang, S. Huang, Z. Wu, C.F. Guo, Natural Plant Materials as Dielectric Layer for Highly Sensitive Flexible Electronic Skin, Small 14 (35) (2018) 1801657.
[17] Y.J. Guo, S. Gao, W.J. Yue, C.W. Zhang, Y. Li, Anodized Aluminum Oxide-Assisted Low-Cost Flexible Capacitive Pressure Sensors Based on Double-Sided Nanopillars by a Facile Fabrication Method, ACS Appl. Mater. Inter. 11 (51) (2019) 48594–48603, https://doi.org/10.1021/acsami.9b17966.
[18] C.M. Boutry, A. Nguyen, Q.O. Lawal, A. Chortos, S. Rondeau-Gagne, Z.N. Bao, A Sensitive and Biodegradable Pressure Sensor Array for Cardiovascular Monitoring, Adv. Mater. 27 (43) (2015) 6954-+, https://doi.org/10.1002/adma.201502535.
[19] Y. Wan, Z. Qiu, Y. Hong, Y. Wang, J. Zhang, Q. Liu, Z. Wu, C.F. Guo, A Highly Sensitive Flexible Capacitive Tactile Sensor with Sparse and High-Aspect-Ratio Microstructures, Adv. Electron. Mater. 4 (4) (2018) 1700586.
[20] Y. Xiong, Y. Shen, L. Tian, Y. Hu, P. Zhu, R. Sun, C.-P. Wong, A flexible, ultra-highly sensitive and stable capacitive pressure sensor with convex microarrays for motion and health monitoring, Nano Energy 70 (2020) 104436.
[21] S. Chen, L.J. Sun, X.J. Zhou, Y.F. Guo, J.C. Song, S.H. Qian, Z.H. Liu, Q.B. Guan, E. M. Jeffries, W.G. Liu, Y.D. Wang, C.L. He, Z.W. You, Mechanically and biologically skin-like elastomers for bio-integrated electronics, Nat. Commun. 11 (1) (2020), https://doi.org/10.1038/s41467-020-14446-2.
[22] H. Jin, M.O.G. Nayeem, S. Lee, N. Matsuhisa, D. Inoue, T. Yokota, D. Hashizume, T. Someya, Highly Durable Nanofiber-Reinforced Elastic Conductors for Skin-Tight Electronic Textiles, ACS Nano 13 (7) (2019) 7905–7912, https://doi.org/10.1021/acsnano.9b02297.
[23] R.J. Zhu, D.L. Fan, W.Y. Wu, C.S. He, G.J. Xu, J.S. Dai, H.Q. Wang, Soft Robots for Cluttered Environments Based on Origami Anisotropic Stiffness Structure (OASS) Inspired by Desert Iguana, Adv. Intell. Syst.-Ger. (2023), https://doi.org/10.1002/aisy.202200301.
[24] Z. Lin, L.S. Novelino, H. Wei, N.A. Alderete, G.H. Paulino, H.D. Espinosa, S. Krishnaswamy, Folding at the Microscale: Enabling Multifunctional 3D Origami-Architected Metamaterials, Small 16 (35) (2020) 2002229.
[25] X.Y. Yin, Y. Zhang, X.B. Cai, Q.Q. Guo, J. Yang, Z.L. Wang, 3D printing of ionic conductors for high-sensitivity wearable sensors, Mater. Horiz. 6 (4) (2019) 767–780, https://doi.org/10.1039/c8mh01398e.
[26] X.-Y. Yin, Y. Zhang, J. Xiao, C. Moorlag, J. Yang, Monolithic Dual-Material 3D Printing of Ionic Skins with Long-Term Performance Stability, Adv. Funct. Mater. 29 (39) (2019) 1904716.
[27] Z.Y. Lei, Q.K. Wang, P.Y. Wu, A multifunctional skin-like sensor based on a 3D printed thermo-responsive hydrogel, Mater. Horiz. 4 (4) (2017) 694–700, https://doi.org/10.1039/c7mh00262a.
[28] J. Li, H. Godaba, J. Zhu, Paper-based origami transducer capable of both sensing and actuation, Extreme Mech. Lett. 49 (2021) 101507.
[29] S. Chen, B. Zhuo, X. Guo, Large Area One-Step Facile Processing of Microstructured Elastomeric Dielectric Film for High Sensitivity and Durable Sensing over Wide Pressure Range, ACS Appl. Mater. Interfaces 8 (31) (2016) 20364–20370, https://doi.org/10.1021/acsami.6b05177.
[30] M.S. Kim, Y. Lee, J. Ahn, S. Kim, K. Kang, H. Lim, B.-S. Bae, I. Park, Skin-like Omnidirectional Stretchable Platform with Negative Poisson's Ratio for Wearable Strain-Pressure Simultaneous Sensor, Adv. Funct. Mater. 33 (3) (2023) 2208792.